Spatiotemporal graph states from a single optical parametric oscillator

Rongguo Yang, Jing Zhang, Israel Klich, Carlos González-Arciniegas, and Olivier Pfister

Spatiotemporal graph states from a single optical parametric oscillator

Rongguo Yang and Jing Zhang*

College of Physics and Electronic Engineering, Collaborative Innovation Center of Extreme Optics,
Shanxi University, Taiyuan 030006, P.R. China and
Department of Physics, University of Virginia, 382 McCormick Road, Charlottesville, Virginia 22904-4714, USA

Israel Klich, Carlos González-Arciniegas, and Olivier Pfister†

Department of Physics, University of Virginia, 382 McCormick Road, Charlottesville, Virginia 22904-4714, USA
(Dated: February 16, 2020)

An experimental scheme is proposed for building massively multipartite entangled states using both the spatial and the frequency modes of an optical parametric oscillator. We provide analytical forms of the entangled states using the squeezed eigenmodes of Heisenberg equations, a.k.a. the nullifiers of the corresponding graph state. This scheme can generate, in parallel, several cluster states described by sparsely connected, bicolorable graphs, usable for one-way quantum computing.

I. INTRODUCTION

Quantum entanglement is an elementary and key resource for quantum information and quantum computing [1]. Cluster states, as 2D sparse graph states, are of central importance for one-way quantum computing, be it over discrete variables [2, 3] or continuous variables (CV) [4–6]. It is important to note that CV quantum computing [7] is a valid type of universal quantum computing that features the same exponential speedup [8, 9] as well as a quantum error correction encoding [10] and a fault tolerance threshold [11, 12].

The experimental generation of photonic CV cluster states first used "bottom up" quantum-circuit like approaches [13], based on the Bloch-Messiah decomposition [14] which yielded four-mode [15, 16] and eight-mode [17] cluster states, using several optical parametric oscillators (OPOs) and linear optical transformations. In this approach the number of OPOs is proportional to the number of entangled modes.

An alternative, top down approach was first proposed in the frequency domain [18, 19], then in the time domain [20, 21]. Such an approach requires only one OPO to generate two-mode squeezed states, a.k.a. Einstein-Podolsky-Rosen (EPR) pairs, over the OPO's optical frequency comb or, alternatively, two frequency-degenerate OPOs to generate two-mode squeezed states in temporally pulsed modes. The first proposal featured a square-grid cluster state, universal for quantum computing, but required a single OPO with a triple (but demonstrated [22]) nonlinear medium and, in particular, a complex pump spectrum [23]. Subsequent, simpler proposals for building cluster states sequentially in the time domain [20, 21] were adapted experimentally in the frequency domain to build 15 independent quadripartite square cluster states [24] and one 60-partite, and two 30-partite, one-dimensional cluster states [25]. Note that,

in the latter case, the demonstrated number of entangled qumodes was not limited by the OPO phasematching bandwidth, which extends to $\sim 10^4$ modes [26], but by the tunability of the local oscillator laser in the interferometric squeezing measurements. Another approach used a synchronously pumped OPO to yield a much broader qumode frequency spacing, well suited for parallel quantum processing [27]. In the temporal domain, entangled modes are obtained sequentially, only two or four at a time but the resulting polynomial overhead for quantum processing is offset by scalability, the total number of entangled modes being limited only by the stability of the experiment. One-dimensional cluster states were thus generated over 10^4 [28], then 10^6 [29] modes. Recently, large-scale two-dimensional square-lattice cluster states were generated [30, 31].

In this context, an interesting additional degree of freedom to explore is the transverse spatial one. Continuous-variable entanglement between two spatial modes was realized within one beam [32]. Linear cluster states were produced among different spatial modes and all possible spatial modes of light were copropagated within one beam [33]. The generation of a CV dual-rail cluster state based on an optical spatial mode comb was proposed via a four-wave-mixing process [34]. Proposals were also made for large-scale CV dual-rail cluster state generation involving Laguerre-Gaussian (LG) modes in a large-Fresnel-number degenerate OPO [35], and in a spatial mode comb pumped by two spatial LG modes [36]. A CV square quadripartite cluster state was experimentally produced by multiplexing orthogonal spatial modes in a single optical parametric amplifier (OPA) [37].

In this paper, we consider the process of optical parametric amplification in a single OPO pumped by two LG modes and the parallel generation of entangled graph states in both the frequency and space domains. Laguerre-Gaussian modes, which carry orbital angle momentum due to helical phase, bring about an additional degree of freedom. This paper is organized as follows: In Sec. II, we describe our system and solve its Hamiltonian analytically to calculate the resulting multipartite entanglement using the CV graph state formalism through the
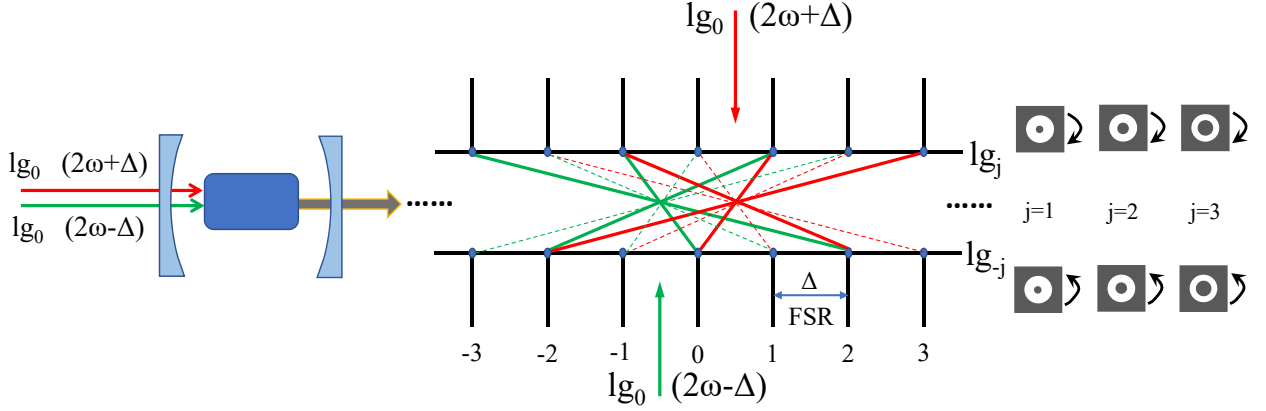
FIG. 1. Schematic of experimental setup. the green and red arrows represent pump modes lg_0 with the frequency $\omega_p = 2\omega \pm \Delta$, the green (red) solid/dashed (generate symmetrically) line connect two modes of down-converted process from the same pump.

G and A adjacency matrices for the $\mathcal{H}$ graph and canonical graph, respectively [19]. In Sec. III, we give numerical illustrations of this result for 8 and 60 modes, and indicate how finite squeezing would affect measurements of weighted-graph states.

II. PHYSICAL SYSTEM AND ANALYTIC SOLUTIONS

In our system, a nonlinear crystal is placed in a self-imaging or large-Fresnel-number cavity, which can be simultaneously resonant for many transverse modes [38], and its transverse eigenmodes are the complete set of LG modes, longitudinal eigenmodes are spaced by the free spectral range (FSR). This specially designed cavity can guarantee simultaneous and sustainable nonlinear interaction and resonance of all the down converted modes [39]. As is shown in Fig.1, the system is pumped by two spatial LG modes lg_0 with frequencies $\omega_p = 2\omega \pm \Delta$, where Δ is the FSR, and $\mu = \pm j$ in lg_μ mode denotes the OAM mode number. Here $j = 0$ for the pump field and $j = 1, 2, 3, ..., m$ for the corresponding downconverted fields. The nonlinear crystal in the cavity is a type I phase-matching crystal whose second order nonlinear coefficient is ξ. The two pump fields of frequency ω_p can be downconverted into signal and idler fields of frequencies $\omega_{s,i} = \omega \pm n\Delta$, $n = 0, 1, 2...$ The nonlinear interaction must satisfy energy conservation ($\omega_p = \omega_s + \omega_i$), phase-matching ($\vec{k}_p = \vec{k}_s + \vec{k}_i$) and orbital angular momentum conservation ($\mu_p = 0 = \mu_s + \mu_i$). Each pair of modes connected by a red or green line are from the same optical down conversion process and can form a high-connected entanglement state of optical frequency and spatial modes.

The interaction Hamiltonian of the system is

$$H = i\hbar\xi \sum_{i=-n}^{n} \sum_{j=1}^{m} \{ G_{(-i,\pm j),(-1+i,\mp j)} \hat{b}_{-1,0} \hat{a}^\dagger_{-i,\pm j} \hat{a}^\dagger_{-1+i,\mp j}$$
$$+ G_{(i,\pm j),(1-i,\mp j)} \hat{b}_{1,0} \hat{a}^\dagger_{i,\pm j} \hat{a}^\dagger_{1-i,\mp j} \} + H.c., \quad (1)$$

where the G matrix element is 1 when the parametric process exists and 0 otherwise. $\hat{b}_{1,0}$ and $\hat{b}_{-1,0}$ denote the annihilation operators of the two pump modes with frequency $2\omega \pm \Delta$, respectively, their first and second index corresponding to the frequency and OAM number, respectively. The pump $\hat{b}_{-1,0}$ can thus produce $\hat{a}_{-i,\pm j}$ and $\hat{a}_{-1+i,\mp j}$ by down-conversion process, and the pump $\hat{b}_{1,0}$ can produce $\hat{a}_{i,\pm j}$ and $\hat{a}_{1-i,\mp j}$.

Note that the spatial and spectral properties of the eigenmodes are reasonably independent, the Gouy phase being the same for spatial modes of same order in the absence of dispersion.

Here, we only consider the first order LG modes, $j = 1$, $\mu = \pm 1$, in the down-conversion modes; similar reasoning can be used when considering higher order modes $j > 1$. The physical system and corresponding $\mathcal{H}$ graph are shown in Fig.2. In Fig. 2(a), certain upper modes of lg_1 and certain lower modes of lg_{-1} are connected by the red (green) lines, and the cross point of all red (green) lines corresponds to the red (green) pump. In Fig. 2(b), one can see the relation and structure of the down-converted fields clearly. Actually, the symmetric cluster state array can be produced simultaneously, as is shown by dashed line in Fig.1. For convenience, we rename these modes from 1 to $N = 2n$ (we always consider a even number of modes). According to the interaction Hamiltonian and the renamed modes, the G matrix can
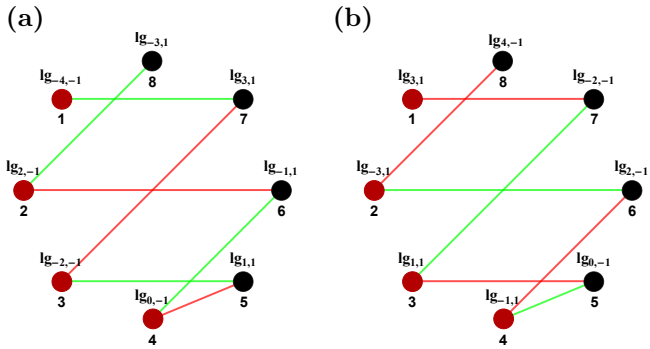
FIG. 2. (a) Physical picture of the mode entanglement with different pumps. Downconverted modes (j=1 only) from each pump are connected with red and green arrows. (b) $\mathcal{H}$ graph.

be written as

$$
G = \left(\begin{array}{ccc} & \vdots & \\ & \begin{matrix} 0 & 0 & 0 & 0 & 0 & 0 & 1 & 0 \\ 0 & 0 & 0 & 0 & 0 & 1 & 0 & 1 \\ 0 & 0 & 0 & 0 & 1 & 0 & 1 & 0 \\ 0 & 0 & 0 & 0 & 1 & 1 & 0 & 0 \\ 0 & 0 & 1 & 1 & 0 & 0 & 0 & 0 \\ 0 & 1 & 0 & 1 & 0 & 0 & 0 & 0 \\ 1 & 0 & 1 & 0 & 0 & 0 & 0 & 0 \\ 0 & 1 & 0 & 0 & 0 & 0 & 0 & 0 \end{matrix} & \\ & \vdots & \end{array} \right) \cdots . \quad (2)
$$

for any N-mode state. This matrix can be seen as the adjacency matrix of the $\mathcal{H}$(amiltonian) graph, which is bipartite, or bicolorable, meaning that all qumodes are distributed into two sets with no any two qumodes in either set interacting with each other. It should also be noted that Eq. (2) assumes that the phasematching bandwidth of the OPO has a flat-top shape and "turns off" sharply between the last mode in the considered set and its neighbor. In practice, while the former was experimentally demonstrated in periodically poled KTP [25, 26], the latter is, however, not doable and the coupling to wing modes will necessarily be tapering. However, such boundary imperfections can be considered confined to their location, the boundary, if the canonical graph (see below) is sparse, i.e., local, enough. (In the case of complete graphs, i.e., GHZ states, this can be more of a problem.)

The spectrum of this graph can be derived analytically

(see Appendix for details). The eigenvalues of G are

$$
\lambda_k = \pm 2 \left| \cos \frac{k\pi}{2n+1} \right|, \quad (3)
$$

where $k = 1, 2, 3, ..., n$. Because there are n eigenvalues with each sign, the solutions of the Heisenberg equations are n amplitude-quadrature squeezed and n phase-quadrature squeezed eigenmodes, of squeezing factor $\exp(\lambda_k \xi t)$, t being the Hamiltonian interaction time (or cavity lifetime in this simplified model).

For pure two-mode squeezing Hamiltonians such as that of Eq. (1), the multipartite state resulting from the quantum evolution can always be expressed as a cluster state [19]. This means that the N eigenmodes always have the following quantum standard deviation

$$
\Delta[\vec{P}(t) - A\vec{Q}(t)] \propto e^{-\xi t}, \quad (4)
$$

where $\vec{P}(t) = [P_1(t),...,P_N(t)]^T$, $\vec{Q}(t) = [Q_1(t),...,Q_N(t)]^T$, $P_j = (a_j - a_j^\dagger)/(i\sqrt{2})$, $Q_j = (a_j + a_j^\dagger)/\sqrt{2}$, and A is the adjacency matrix of the canonical cluster graph, which is the CV equivalent [4] of a qubit cluster state [2]. In order to determine the corresponding cluster state, we need to derive this adjacency matrix. This can be done analytically (see Appendix for details), yielding

$$
A = \left(\begin{array}{cc} 0 & S^T B^T S J \\ J S^T B S & 0 \end{array} \right), \quad (5)
$$

where J is the anti-diagonal identity matrix, S is a permutation matrix, and B is constructed from the eigenvectors of G. The matrices B in (5) are derived explicitly in the appendix, with the result:

$$
B_{ij} = \frac{(-1)^{i+j+n}}{1+2n} \left[\frac{1}{\cos(\frac{(i-j)\pi}{1+2n})} + \frac{1}{\cos(\frac{(i+j-1)\pi}{1+2n})} \right]. \quad (6)
$$

The matrices S and J have the matrix elements $S_{ij} = \delta_{j,2i-1} + \delta_{j,2i-2n-2}$ and $J_{ij} = \delta_{i,n-j+1}$.

The form (5) of A shows that the resulting cluster graph is bicolorable.

III. ILLUSTRATIVE EXAMPLES

In this section, we give numerical examples of the obtained graph states for two different scales.

A. Small scale

The possible $\mathcal{H}$ graphs for an eight-mode state are shown in Fig.3, with each vertex corresponding to a different qumode. Red and green lines correspond to different pumps. It is interesting to note that both these

FIG. 3. The two possible $\mathcal{H}$ graphs for an eight-mode state.

graphs have the same linear chain structure, i.e., that G is a Hankel-like, and even centrosymmetric, matrix. As shown in the previous section, the canonical (e.g., cluster) graph state is obtained from its adjacency matrix A, calculated from Eq. (5) and also using the method outlined in Ref. 19, and displayed in Fig.4(a). This matrix corresponds, in general to a weighted complete bicolorable graph, drawn in Fig.4(b).
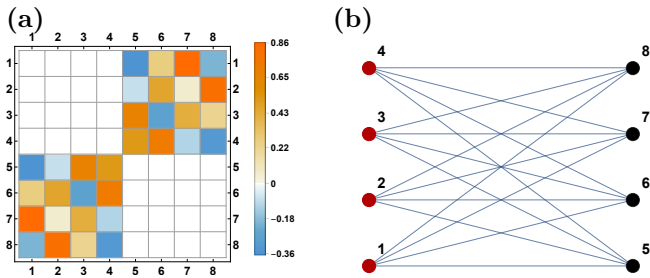

FIG. 4. (a), A matrix and, (b), corresponding canonical graph for an 8-mode state.

B. Large scale

In order to gain perspective on the overall structure—if any—of the graph state, we now expand to an arbitrary larger, yet computable, number of modes, e.g. 60 modes. Note that the maximum mode number depends on the ratio of the phasematching spectral bandwidth with the FSR. The phasematching bandwidth in PPKTP can be very large, on the order of 10 THz for some interactions with a 532 nm pump wavelength, as was calculated and measured in Ref. 26. For a typical FSR on the order of 1 GHz, this can yield $\sim 10^4$ qumodes. Figure 5 displays the A matrix for 60 modes. Besides its aforementioned bipartite structure, A also has a skew-symmetric structure that clearly mirrors that of G, Eq. (2) [40]. Although A is nominally a complete bicolorable graph (i.e., nodes 1 to 30 are not linked to one another but are all linked to all of the nodes 31 to 60), it is also strongly weighted, as the absolute values of the nonzero A matrix

elements range from orders 10^{-4} to 1. A natural question is then to ask what is the physical significance, and even the relevance, of these very weak edges. An intuitive answer to this question is to examine the edge weight relative to the available squeezing [41]: in a nutshell, it is well known that the edge between two qumodes describes their quantum correlations, as evidenced by the formal equivalence between a two-mode cluster state and a two-mode squeezed state [21]. The squeezing parameter ξt used in experimentally realizing cluster entanglement then naturally serves as the noise floor for observing quantum correlations between modes and a rule of thumb is that an edge of weight ε, i.e., an element of A of value ε, will only be relevant if the squeezing is large enough, i.e., if $\varepsilon \gtrsim \exp(-2\xi t)$; otherwise the quantum correlations due to the edge of weight ε will be buried in the squeezed quantum noise, therefore unobservable and, for all intents and purposes, nonexistent.

With this criterion in mind, we examine matrix A again after rounding down all elements below a certain threshold to zero, the thresholds being chosen to correspond to realistic values of squeezing: Fig.6 displays the results of such "graph pruning" for three different, contiguous threshold ranges. Because the graphs are regular, save for local imperfections at the boundaries (chains' ends), we only displayed central sections to clearly highlight changes in graph valence and structure. It is remarkable that the lowest squeezing amounts already yield a 1D cluster wire spanning all qumodes in the considered set, a universal structure for single-qumode quantum processing. As the squeezing increases, the graphs gain "width" while retaining the 1D structure of the main two skew diagonals of the A matrix, becoming a ladder structure then a spiraling wire overlapping with three parallel wires. Note the current record of optical squeezing is -15 dB [42]. Being a cluster state, the graph can be
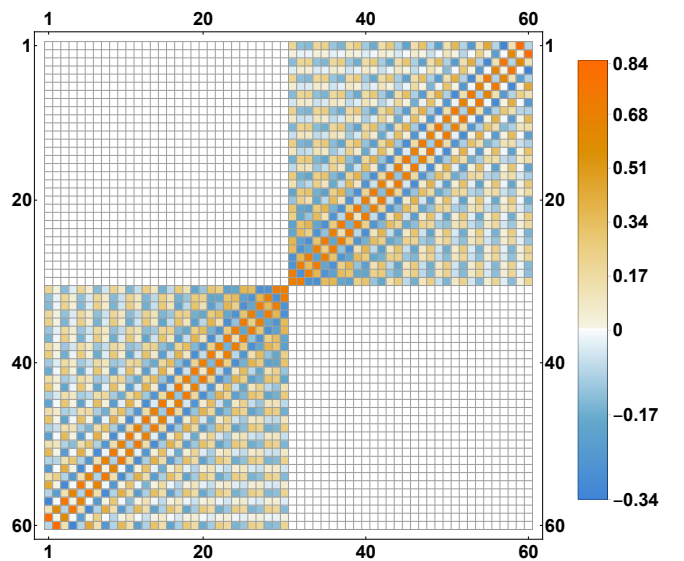
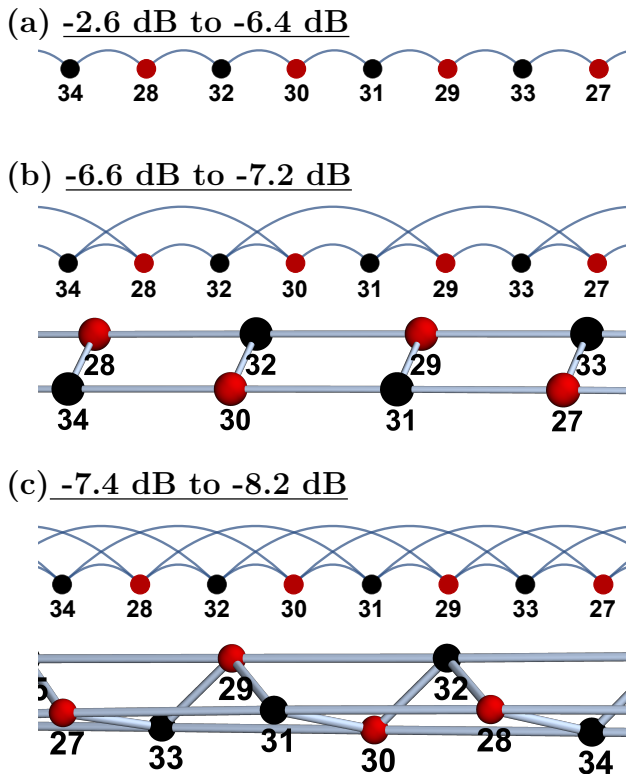

FIG. 5. The A matrix for 60 modes.

(a) -2.6 dB to -6.4 dB

(b) -6.6 dB to -7.2 dB

(c) -7.4 dB to -8.2 dB

FIG. 6. Graph states obtained from A with increasing squeezing, by neglecting A elements below threshold. (a), threshold range 0.55-0.23 (squeezing range -2.6 dB to -6.4 dB); (b) threshold range 0.22-0.19 (squeezing range -6.6 dB to -7.2 dB); (c) threshold range 0.18-0.15 (squeezing range -7.4 dB to -8.2 dB).

"trimmed" to a desired shape by measuring out the unwanted vertices [2, 3]. Moreover, such structures has been shown to enable additional quantum processing options, also decided by measurements and feedforward within the model of one-way quantum computing [43, 44].

IV. CONCLUSION

We have shown that a single OPO specifically engineered to add spatial degrees of freedom to the usual frequency ones of its resonant modes, can generate, in one fell swoop, sophisticated large-scale multipartite cluster states. We have derived analytic solutions for the state and have examined the physical significance of the edge weighting of the generated graph state, in terms of the available experimental squeezing. Three essential points should be noted:

(i) These graphs being cluster states, they can be shaped and trimmed by measurements of undesired connected vertices.

(ii) Measurements and feedforward can also be used in a more elaborate manner, by taking advantage

of the additional graph edge structure on a 1D or 2D backbone for implementing additional, arbitrary quantum operations [43, 44].

(iii) Such cluster states can also be produced in parallel, by use of higher order spatial modes $lg_{\pm2}, lg_{\pm3}, \cdots$ Although the effective coupling strength ξ will initially be expected to be smaller for these modes due to the smaller overlap between the pump, signal and idler modes [35, 36], ξ can be effectively enhanced by introducing a specially designed nonlinear crystal structure for matching the property of LG modes and the structured transverse mode of pump [45].

Appendix A: Analytical expressions of the A and G matrices

Here we provide the details on how we obtain the eigenvalues/eigenvectors of the G matrix and the analytical expression of the A matrix.

1. Eigenvalues and eigenvectors of the G matrix

Let us write the $2n \times 2n$ G matrix, Eq. (2), as:

$$G = \begin{pmatrix} 0 & Q \\ Q^T & 0 \end{pmatrix}. \quad (A1)$$

where:

$$Q = \begin{pmatrix} \cdots & 0 & 0 & 1 & 0 \\ 0 & 0 & \cdots & 0 & 1 \\ 0 & 1 & \cdots & \cdots & 0 \\ 1 & 0 & 1 & 0 & 0 \\ 1 & 1 & 0 & 0 & \cdots \end{pmatrix} \quad (A2)$$

Let $M = QQ^T$. Note that G^2 has the form:

$$G^2 = \begin{pmatrix} QQ^T & 0 \\ 0 & Q^TQ \end{pmatrix} = \begin{pmatrix} M & 0 \\ 0 & JMJ \end{pmatrix} \quad (A3)$$

where J is the anti-diagonal identity matrix, $J_{ij} = \delta_{i,n-j+1}$. Here

$$M = \begin{pmatrix} 1 & 0 & 1 & 0 & ... & 0 \\ 0 & 2 & 0 & 1 & 0 & ... \\ 1 & 0 & 2 & 0 & ... & 0 \\ 0 & 1 & 0 & ... & 0 & 1 \\ ... & 0 & ... & 0 & 2 & 1 \\ 0 & ... & 0 & 1 & 1 & 2 \end{pmatrix} \qquad (A4)$$

It is possible to transform M into a tridiagonal matrix M' by a permutation of the indices, getting:

$$SMS^T \equiv M' = \begin{pmatrix} 1 & 1 & 0 & 0 & 0 & ... \\ 1 & 2 & 1 & 0 & 0 & 0 \\ 0 & 1 & 2 & ... & 0 & 0 \\ 0 & 0 & ... & ... & 1 & 0 \\ 0 & 0 & 0 & 1 & 2 & 1 \\ ... & 0 & 0 & 0 & 1 & 2 \end{pmatrix} \qquad (A5)$$

where the permutation matrix S is defined by:

$$(S^T \vec{\alpha})_j = \begin{cases} \alpha_i & j = 2i-1 \\ \alpha_{n-i+1} & j = 2i \end{cases} \qquad (A6)$$

As an example, for $n = 12$, the S matrix has the form:

$$S = \begin{pmatrix} 1 & 0 & 0 & 0 & 0 & 0 \\ 0 & 0 & 1 & 0 & 0 & 0 \\ 0 & 0 & 0 & 0 & 1 & 0 \\ 0 & 0 & 0 & 0 & 0 & 1 \\ 0 & 0 & 0 & 1 & 0 & 0 \\ 0 & 1 & 0 & 0 & 0 & 0 \end{pmatrix}. \qquad (A7)$$

The matrix M' is a simple tridiagonal matrix that has known eigenvalues and eigenvectors [46]:

$$(v_k)_j = \frac{2}{\sqrt{2n+1}} \sin \frac{k(2j-1)\pi}{2n+1} \qquad (A8)$$

$$\lambda_k^2 = 4 \cos^2 \frac{k\pi}{2n+1}. \qquad (A9)$$

Since the eigenvalues of M and JMJ are the same as of M''s, we conclude that the eigenvalues of G^2 are λ_k^2, with a double degeneracy, and for the matrix G the eigenvalues are

$$\lambda_k = \pm 2 \left| \cos \frac{k\pi}{2n+1} \right|. \qquad (A10)$$

We note that

$$[G, \mathcal{J}] = 0 \qquad (A11)$$

$$\mathcal{J} = \begin{pmatrix} 0 & J \\ J & 0 \end{pmatrix} \qquad (A12)$$

and therefore the eigenvectors of G can be chosen as eigenvectors of $\mathcal{J}$ as well, i.e. either symmetric or antisymmetric around the middle. We find that the sym-

metric eigenvectors are given by

$$V_{k,\text{sym}} = \begin{pmatrix} S^T v_k \\ JS^T v_k \end{pmatrix} \qquad (A13)$$

with eigenvalues $(-1)^k \lambda_k$ and the antisymmetric ones are

$$V_{k,\text{asym}} = \begin{pmatrix} S^T v_k \\ -JS^T v_k \end{pmatrix} \qquad (A14)$$

with eigenvalue $(-1)^{k+1} \lambda_k$.

2. Construction of the A matrix.

The A matrix is obtained as follows [19]. First, diagonalize G and separate into positive and negative blocks:

$$G = VDV^T, \quad D = \begin{pmatrix} \lambda_1 & 0 & 0 & 0 & ... & ... \\ 0 & .. & 0 & 0 & ... & ... \\ 0 & 0 & \lambda_n & 0 & 0 & 0 \\ 0 & 0 & 0 & -\lambda_1 & 0 & 0 \\ ... & ... & 0 & 0 & .. & 0 \\ ... & ... & 0 & 0 & 0 & -\lambda_n \end{pmatrix}$$

Then:

$$A = \begin{pmatrix} 0 & A_0 \\ A_0^T & 0 \end{pmatrix}$$

where

$$A_0 = -V_{12} (V_{22})^{-1} ; \quad V = \begin{pmatrix} V_{11} & V_{12} \\ V_{21} & V_{22} \end{pmatrix}$$

Fortunately, in our case, V has a simple form that allows the inversion of the relevant block.

To construct V we use the eigenvectors (A13) and (A14) as column vectors, which will automatically yield a diagonalization of G. It is only left to order them so that the first columns correspond to positive eigenvalues and the second half of columns correspond to negative eigenvalues. To separate between positive and negative eigenvectors, we choose the ordering: $V_{1,asym}, V_{2,sym}, V_{3,asym}, ...$

Concretely, let

$$V_{11} = S^T(v_1, v_2, .., v_n) \qquad (A15)$$

Then our final form is of the form:

$$V = \frac{1}{\sqrt{2}} \begin{pmatrix} V_{11} & V_{11} \\ JV_{11}L & -JV_{11}L \end{pmatrix} \qquad (A16)$$

where $L = diagonal(-1, 1, -1, 1, ...)$ chooses the signs of the second half of columns in V to correspond to the order of $asymmetric, symmetric, asymmetric, symmetric, ...$ specified above.

The block $V_{22} = -JV_{11}L$ is clearly an orthogonal ma-

trix, and we wind up with:

$$A_0 = -V_{12} \left(V_{22}\right)^{-1} = V_{11} L V_{11}^T J = S^T B^T S J \quad \text{(A17)}$$

where B is built from the eigenvectors (A8):

$$B_{ij} = \frac{-4}{1+2n} \sum_{k=1}^{n} (-1)^k \sin \frac{k(2i-1)\pi}{2n+1} \sin \frac{k(2j-1)\pi}{2n+1} \tag{A18}$$

$$= \frac{(-1)^{i+j+n}}{1+2n} \left[\frac{1}{\cos(\frac{(i-j)\pi}{1+2n})} + \frac{1}{\cos(\frac{(i+j-1)\pi}{1+2n})} \right], \tag{A19}$$

where $i = 1, 2..., n; j = 1, 2, ..., n$. Finally, the A matrix is eq A:

$$A = \begin{pmatrix} 0 & S^T B^T S J \\ J S^T B S & 0 \end{pmatrix}. \tag{A20}$$

[1] M. A. Nielsen and I. L. Chuang, *Quantum computation and quantum information* (Cambridge University Press, Cambridge, U.K., 2000).

[2] H. J. Briegel and R. Raussendorf, Persistent entanglement in arrays of interacting particles, Phys. Rev. Lett. **86**, 910 (2001).

[3] R. Raussendorf and H. J. Briegel, A one-way quantum computer, Phys. Rev. Lett. **86**, 5188 (2001).

[4] J. Zhang and S. L. Braunstein, Continuous-variable Gaussian analog of cluster states, Phys. Rev. A **73**, 032318 (2006).

[5] N. C. Menicucci, P. van Loock, M. Gu, C. Weedbrook, T. C. Ralph, and M. A. Nielsen, Universal quantum computation with continuous-variable cluster states, Phys. Rev. Lett. **97**, 110501 (2006).

[6] M. Gu, C. Weedbrook, N. C. Menicucci, T. C. Ralph, and P. van Loock, Quantum computing with continuous-variable clusters, Phys. Rev. A **79**, 062318 (2009).

[7] O. Pfister, Continuous-variable quantum computing in the quantum optical frequency comb, Journal of Physics B: Atomic, Molecular and Optical Physics **53**, 012001 (2020).

[8] S. Lloyd and S. L. Braunstein, Quantum computation over continuous variables, Phys. Rev. Lett. **82**, 1784 (1999).

[9] S. D. Bartlett, B. C. Sanders, S. L. Braunstein, and K. Nemoto, Efficient classical simulation of continuous variable quantum information processes, Phys. Rev. Lett. **88**, 097904 (2002).

[10] D. Gottesman, A. Kitaev, and J. Preskill, Encoding a qubit in an oscillator, Phys. Rev. A **64**, 012310 (2001).

[11] N. C. Menicucci, Fault-tolerant measurement-based quantum computing with continuous-variable cluster states, Phys. Rev. Lett. **112**, 120504 (2014).

[12] K. Fukui, A. Tomita, A. Okamoto, and K. Fujii, High-threshold fault-tolerant quantum computation with analog quantum error correction, Phys. Rev. X **8**, 021054 (2018).

[13] P. van Loock, C. Weedbrook, and M. Gu, Building Gaussian cluster states by linear optics, Phys. Rev. A **76**, 032321 (2007).

[14] S. L. Braunstein, Squeezing as an irreducible resource, Phys. Rev. A **71**, 055801 (2005).

[15] X. Su, A. Tan, X. Jia, J. Zhang, C. Xie, and K. Peng, Experimental preparation of quadripartite cluster and Greenberger-Horne-Zeilinger entangled states for continuous variables, Phys. Rev. Lett. **98**, 070502 (2007).

[16] M. Yukawa, R. Ukai, P. van Loock, and A. Furusawa, Experimental generation of four-mode continuous-variable cluster states, Phys. Rev. A **78**, 012301 (2008).

[17] X. Su, Y. Zhao, S. Hao, X. Jia, C. Xie, and K. Peng, Experimental preparation of eight-partite cluster state for photonic qumodes, Opt. Lett. **37**, 5178 (2012).

[18] O. Pfister, S. Feng, G. Jennings, R. Pooser, and D. Xie, Multipartite continuous-variable entanglement from concurrent nonlinearities, Phys. Rev. A **70**, 020302 (2004).

[19] N. C. Menicucci, S. T. Flammia, H. Zaidi, and O. Pfister, Ultracompact generation of continuous-variable cluster states, Phys. Rev. A **76**, 010302(R) (2007).

[20] N. C. Menicucci, X. Ma, and T. C. Ralph, Arbitrarily large continuous-variable cluster states from a single quantum nondemolition gate, Phys. Rev. Lett. **104**, 250503 (2010).

[21] N. C. Menicucci, S. T. Flammia, and P. van Loock, Graphical calculus for Gaussian pure states, Phys. Rev. A **83**, 042335 (2011).

[22] M. Pysher, A. Bahabad, P. Peng, A. Arie, and O. Pfister, Quasi-phase-matched concurrent nonlinearities in periodically poled KTiPO$_4$ for quantum computing over the optical frequency comb, Opt. Lett. **35**, 565 (2010).

[23] N. C. Menicucci, S. T. Flammia, and O. Pfister, One-way quantum computing in the optical frequency comb, Phys. Rev. Lett. **101**, 130501 (2008).

[24] M. Pysher, Y. Miwa, R. Shahrokhshahi, R. Bloomer, and O. Pfister, Parallel generation of quadripartite cluster entanglement in the optical frequency comb, Phys. Rev. Lett. **107**, 030505 (2011).

[25] M. Chen, N. C. Menicucci, and O. Pfister, Experimental realization of multipartite entanglement of 60 modes of a quantum optical frequency comb, Phys. Rev. Lett. **112**, 120505 (2014).

[26] P. Wang, W. Fan, and O. Pfister, Engineering large-scale entanglement in the quantum optical frequency comb: influence of the quasiphasematching bandwidth and of

dispersion, arXiv:1403.6631 [physics.optics] (2014).

[27] J. Roslund, R. Medeiros de Araújo, S. Jiang, C. Fabre, and N. Treps, Wavelength-multiplexed quantum networks with ultrafast frequency combs, Nat. Photon. **8**, 109 (2014).

[28] S. Yokoyama, R. Ukai, S. C. Armstrong, C. Sornphiphatphong, T. Kaji, S. Suzuki, J. Yoshikawa, H. Yonezawa, N. C. Menicucci, and A. Furusawa, Ultra-large-scale continuous-variable cluster states multiplexed in the time domain, Nat. Photon. **7**, 982 (2013).

[29] J.-i. Yoshikawa, S. Yokoyama, T. Kaji, C. Sornphiphatphong, Y. Shiozawa, K. Makino, and A. Furusawa, Invited article: Generation of one-million-mode continuous-variable cluster state by unlimited time-domain multiplexing, APL Photonics **1**, 060801 (2016).

[30] W. Asavanant, Y. Shiozawa, S. Yokoyama, B. Charoensombutamon, H. Emura, R. N. Alexander, S. Takeda, J.-i. Yoshikawa, N. C. Menicucci, H. Yonezawa, and A. Furusawa, Generation of time-domain-multiplexed two-dimensional cluster state, Science **366**, 373 (2019), https://science.sciencemag.org/content/366/6463/373.full.pdf.

[31] M. V. Larsen, X. Guo, C. R. Breum, J. S. Neergaard-Nielsen, and U. L. Andersen, Deterministic generation of a two-dimensional cluster state, Science **366**, 369 (2019), https://science.sciencemag.org/content/366/6463/369.full.pdf.

[32] J. Janousek, K. Wagner, J.-F. Morizur, N. Treps, P. K. Lam, C. C. Harb, and H.-A. Bachor, Spatial multimode entanglement within one laser beam, Nat. Photonics **3**, 399 (2009).

[33] S. Armstrong, J.-F. Morizur, J. Janousek, B. Hage, N. Treps, P. K. Lam, and H.-A. Bachor, Programmable multimode quantum networks, Nat. Commun. **3:1026**, 1 (2012).

[34] R. Pooser and J. Jing, Continuous-variable cluster-state generation over the optical spatial mode comb, Phys. Rev. A **90**, 043841 (2014).

[35] R. Yang, J. Wang, J. Zhang, K. Liu, and J. Gao, Generation of continuous-variable spatial cluster entangled states in optical mode comb, J. Opt. Soc. Am. B **33**, 2424 (2016).

[36] J. Zhang, G. Pagano, P. W. Hess, A. Kyprianidis, P. Becker, H. Kaplan, A. V. Gorshkov, Z. X. Gong, and C. Monroe, Observation of a many-body dynamical phase transition with a 53-qubit quantum simulator, Nature **551**, 601 EP (2017).

[37] C. Cai, L. Ma, J. Li, H. Guo, K. Liu, H. Sun, R. Yang, and J. Gao, Generation of a continuous-variable quadripartite cluster state multiplexed in the spatial domain, Photon. Res. **6**, 479 (2018).

[38] B. Chalopin, F. Scazza, C. Fabre, and N. Treps, Multimode nonclassical light generation through the optical-parametric-oscillator threshold, Phys. Rev. A **81**, 061804 (2010).

[39] C. Navarrete-Benlloch, G. J. de Valcárcel, and E. Roldán, Generating highly squeezed hybrid laguerre-gauss modes in large-fresnel-number degenerate optical parametric oscillators, Phys. Rev. A **79**, 043820 (2009).

[40] Note that it is well known [47] that $A = G$ if $G^2 = \mathbb{1}$, but that isn't the case here.

[41] X. Zhu, C.-H. Chang, C. González-Arciniegas, J. Higgins, A. Pe'er, and O. Pfister, Cluster state engineering by phase modulation of the quantum optical frequency comb, arXiv:1912.11215 [quant-ph] (2020).

[42] H. Vahlbruch, M. Mehmet, K. Danzmann, and R. Schnabel, Detection of 15 dB squeezed states of light and their application for the absolute calibration of photoelectric quantum efficiency, Phys. Rev. Lett. **117**, 110801 (2016).

[43] R. N. Alexander, S. C. Armstrong, R. Ukai, and N. C. Menicucci, Noise analysis of single-mode gaussian operations using continuous-variable cluster states, Phys. Rev. A **90**, 062324 (2014).

[44] R. N. Alexander and N. C. Menicucci, Flexible quantum circuits using scalable continuous-variable cluster states, Phys. Rev. A **93**, 062326 (2016).

[45] G. B. Alves, R. F. Barros, D. S. Tasca, C. E. R. Souza, and A. Z. Khoury, Conditions for optical parametric oscillation with a structured light pump, Phys. Rev. A **98**, 063825 (2018).

[46] W.-C. Yueh, Eigenvalues of several tridiagonal matrices, Applied mathematics e-notes **5**, 210 (2005).

[47] H. Zaidi, N. C. Menicucci, S. T. Flammia, R. Bloomer, M. Pysher, and O. Pfister, Entangling the optical frequency comb: simultaneous generation of multiple 2x2 and 2x3 continuous-variable cluster states in a single optical parametric oscillator, Laser Phys. **18**, 659 (2008), revised version at http://arxiv.org/pdf/0710.4980v3.